the two interpretations. However, since ΔE_1 and ΔE_2 processes are observed in the crystalline state where dissociation is also likely to be hindered, we suspect that in the polymer matrix the ^{3}d-d state is simply not accessed in the temperature range investigated.

Conclusions

Photolysis of $[Ru(trpy)(bpy)(NCCH_3)]^{2+}$ dissolved in acetonitrile solutions containing various pyridine derivatives leads to substitution of the acetonitrile ligand by the pyridine. A quantum yield of about 0.0013 can be measured for pyridine and 4-phenylpyridine, while for the sterically hindered 2-methylpyridine the quantum yield is increased approximately 2-fold. These results are incompatible with an associative mechanism of substitution, but they can be reconciled with a dissociative mechanism. In the case of 2-methylpyridine, the increase in quantum yield may reflect a difference in solvation of the entering nucleophile. Previous evidence for a dissociative mechanism in the photosubstitution chemistry of a ruthenium(II) polypyridine complex is available from studies of the photoanation of $[Ru(bpy)_2(py)_2]^{2+}$ in methylene chloride, where the quantum yield for replacement of the first pyridine was found to be independent of the anion.[44] The quantum yields for substitution are low for $[Ru(trpy)(bpy)(NCCH_3)]^{2+}$ despite the fact that the temperature dependence of the luminescence lifetime reveals that there is only a modest barrier (ca. 1500 cm^{-1}) separating the emissive ^{3}CT state from the reactive ^{3}d-d state. Undoubtedly, the yields are attenuated by the fact that the solvent competes for the empty coordination site of the putative five-coordinate intermediate. In addition, dissociation of a terminal Ru-N bond of the trpy and/or bpy ligand in place of the acetonitrile ligand would be expected to lead to no net reaction, since ring closure and regeneration of the original complex is highly favored. Finally, the product complex $[Ru(trpy)(bpy)(py)]^{2+}$ has been structurally characterized as the PF_6^- salt by X-ray crystallography. There is evidence for steric strain in the coordination sphere of ruthenium in the form of a long bond to the pyridine nitrogen and asymmetric coordination of the bpy ligand.

Acknowledgment. This research was supported by NSF Grant No. CHE-8719538. We are indebted to Dan Severance, who did most of the work involved with the AM1 calculation.

Supplementary Material Available: For $[Ru(trpy)(bpy)(py)](PF_6)_2 \cdot (CH_3)_2CO$, tables listing positional parameters and their estimated standard deviations, general temperature factor expressions, bond distances, and bond angles, torsion angles, and least-squares planes along with their dihedral angles (36 pages); a table of calculated and observed structure factors (26 pages). Ordering information is given on any current masthead page.

(43) Juris, A.; Balzani, V.; Barigelletti, F.; Campagna, S.; Belser, P.; von Zelewsky, A. *Coord. Chem. Rev.* **1988**, *84*, 85-277.
(44) Durham, B.; Walsh, J. L.; Carter, C. L.; Meyer, T. J. *Inorg. Chem.* **1980**, *19*, 860-865.

Contribution from the Department of Chemistry,
Frick Laboratory, Princeton University, Princeton, New Jersey 08544-1009

Surface-Attached $[(NC)_5Fe(CN)Pt(NH_3)_4(NC)Fe(CN)_5]^{4-}$: A Study in the Electrochemical and Photochemical Control of Surface Morphology

Brian W. Pfennig and Andrew B. Bocarsly*

Received July 3, 1990

The $[Pt(NH_3)_4]_2^{4+}$ salt of $[(NC)_5Fe^{II}(CN)Pt^{IV}(NH_3)_4(NC)Fe^{II}(CN)_5]^{4-}$ (I) was electrochemically derivatized on a Ni surface by anodic precipitation as the Ni^{2+} analogue, Ni_2I. The resulting electrode surface was characterized by diffuse-reflectance FTIR spectroscopy and cyclic voltammetry. The cyclic voltammetric response of this species was similar to that of the solution species and was found to be only slightly variant with intercalated cation. However, this noncrystalline surface could be photochemically modified to generate a nickel ferrocyanide lattice, which is electrochemically cation sensitive. The photoinduced crystallization process was monitored by parallel electrochemical and X-ray powder pattern experiments. A mechanism for this transformation is proposed. In a separate set of reactions, it was found that the complex of interest can be electropolymerized onto an inert electrode surface. This process is believed to occur via oxidation of the "$[Fe^{II}Pt^{IV}Fe^{II}]^{4-n}$" anion to form the "$[Fe^{III}Pt^{IV}Fe^{III}]^{2-n}$" dianion, which in turn oxidizes one of the Pt(II) counterions to form the polymeric species "$[Fe^{II}Pt^{IV}]_n$." The spectroscopy and electrochemistry of the polymeric species is discussed.

Introduction

In the past several years, it has been demonstrated that electrochemical processes can be modulated and controlled by chemically modified electrodes.[1] Interest in our group has focused on the mixed-metal cyanometalate family of derivatized electrodes, which are structurally analogous with Prussian Blue. Typically, an anodically unstable metal electrode such as nickel is oxidized in the presence of a complex such as $Fe(CN)_5L^{2-}$. A precipitation reaction follows that leads to the formation of an ordered, cyanide-bridged lattice on the surface of the electrode.[1] We have shown that the charge transfer properties of these surface layers are closely related to the surface morphology. One simple technique for varying the surface structure and thus the electrochemical reactivity in the case of a nickel ferrocyanide surface lattice is to intercalate different alkali-metal cations. This process causes a shift in the surface iron redox potential of about 600 mV when Li^+ intercalation is compared with Cs^+ intercalation.[3,4] Our current focus is on designing and controlling the molecular architecture and therefore the microstructure of these three-dimensional lattices.

We have recently reported the single-crystal X-ray structure of the trinuclear, cyanide-bridged complex $\{[Pt(NH_3)_4]_2^{4+}\}\{[NC)_5Fe^{II}(CN)Pt^{IV}(NH_3)_4(NC)Fe^{II}(CN)_5]^{4-}\} \cdot 9H_2O$ ($[Pt(NH_3)_4]_2I$) shown in Figure 1.[5] This previously unreported complex was serendipitously discovered on an electrode surface while the potential of a nickel ferrocyanide derivatized electrode was cycled in a solution of tetraammineplatinum(II) nitrate and subsequently was prepared as a bulk material via reaction in solution. The $[Pt(NH_3)_4]_2I$ complex is interesting not only as it is a well-characterized molecular model of the nickel-cyanometalate system but also because it exhibits an optical intervalent

* Author to whom correspondence should be addressed.

(1) Bocarsly, A. B.; Sinha, S. *J. Electroanal. Chem. Interfacial Electrochem.* **1982**, *137*, 157 and references therein.
(2) Sinha, S.; Humphrey, B. D.; Bocarsly, A. B. *Inorg. Chem.* **1984**, *23*, 203.
(3) Bocarsly, A. B.; Sinha, S. *J. Electroanal. Chem. Interfacial Electrochem.* **1982**, *140*, 167.
(4) Amos, L. J.; Duggal, A.; Mirsky, E. J.; Ragonesi, P.; Bocarsly, A. B.; Fitzgerald-Bocarsly, P. A. *Anal. Chem.* **1988**, *60*, 245.
(5) Zhou, M.; Pfennig, B. W.; Steiger, J. L.; Van Engen, D.; Bocarsly, A. B. *Inorg. Chem.* **1990**, *29*, 2456.

0020-1669/91/1330-0666$02.50/0 © 1991 American Chemical Society

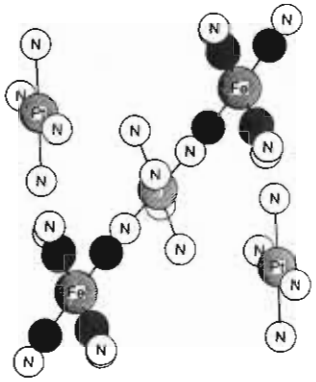

Figure 1. Ball and stick diagram for $\{[Pt(NH_3)_4]_2^{4+}\}\{[(NC)_5Fe^{II}(CN)Pt^{IV}(NH_3)_4(NC)Fe^{II}(CN)_5]^{4-}\}\cdot 9H_2O$. The central atom (label obscured) is platinum and the shaded atoms are carbon.

Fe(II) → Pt(IV) charge-transfer transition that leads to productive photochemistry.[5] The solution cyclic voltammetry of this molecule shows a single redox wave assigned to the two-electron oxidation of the two noninteracting iron moieties. We herein report on the derivatization of this species on a variety of electrode surfaces via either the reaction between $[Pt(NH_3)_4]_2I$ and electrogenerated metal ions or the direct electropolymerization of I and $Pt(NH_3)_4^{2+}$. The resulting surface characterization, electrochemistry, morphology, and photochemistry are discussed.

Experimental Section

$\{[Pt(NH_3)_4]_2^{4+}\}\{[(NC)_5Fe^{II}(CN)Pt^{IV}(NH_3)_4(NC)Fe^{II}(CN)_5]^{4-}\}\cdot 9H_2O$ was prepared by the literature method.[5] The nickelous complex of I (Ni_2I) was synthesized by the reaction of $[Pt(NH_3)_4]_2I$ with excess aqueous $NiCl_2$ and isolated as the precipitate. All other chemicals were reagent grade as purchased from Aldrich and were used without further purification. Derivatization of Ni foils (Alfa, 0.127 mm thickness) was performed by anodizing the nickel at 1.2 V vs SCE for several minutes in the dark in the presence of approximately 50 mM $[Pt(NH_3)_4]_2I$ in deionized water or in the same solution containing 0.1 M $NaNO_3$ supporting electrolyte. Nickel foils were abraded with 150 grit sandpaper, rinsed with distilled water, and wiped dry with a Kimwipe prior to derivatization. Typical electrode coverages were on the order of 10^{-9}–10^{-10} mol/cm^2. SnO_2 on glass electrodes were cleaned with HCl, rinsed with water, wiped dry, and oxidized at 1.2–1.4 V vs SCE in derivatization solutions for 0.5–4 min.

All electrochemical studies employed a Pine Instruments RDE-4 potentiostat equipped with a Houston Instruments Model 2000 XY-recorder. A standard three-electrode configuration with a Pt counter and a SCE was used. Laser irradiation of the electrodes was performed by using a Coherent Innova 70 argon-ion laser at 488 nm. Absorption spectra were recorded on an HP 8450A diode-array spectrometer and FTIR data were obtained on either a Nicolet Model 730 or 800 FTIR spectrophotometer equipped with a diffuse-reflectance sample holder. Spectra were referenced against unreacted pretreated electrodes. Energy-dispersive X-ray analysis (EDX) was performed on a JEOL system with a Princeton Gamma-Tech System III analyzer. Powder X-ray diffraction patterns were obtained with a Phillips 120458/3 water-cooled diffractometer with a type 3253/00 Cu anode operated at 40 kV and 20 mA ($K\alpha$ = 1.5418 Å) at a scan rate of 0.25°/min.

Results and Discussion

Surface Characterization. Species Ni_2I was initially discovered on a nickel ferrocyanide derivatized electrode surface while cycling its potential in $[Pt(NH_3)_4](NO_3)_2$ between 0 and 1 V vs SCE. EDX analysis of the resulting surface is depicted in Figure 2, demonstrating that Pt has in fact been incorporated into the lattice. Figure 3 shows the cyclic voltammograms of a nickel ferrocyanide derivatized electrode whose potential was first cycled in 1 M $NaNO_3$ supporting electrolyte (narrow wave) and then in 1 M $[Pt(NH_3)_4](NO_3)_2$ supporting electrolyte (broad wave). The existence of a cyclic voltammetric wave in the $Pt(NH_3)_4^{2+}$ electrolyte demonstrates that this complex is capable of being transported through the nickel ferrocyanide interfacial lattice. The broad nature of the wave in the Pt solution and shifted redox potential from that in 1 M $NaNO_3$ supporting electrolyte indicate a degree of interfacial reorganization associated with the intercalation of the $Pt(NH_3)_4^{2+}$ species. Figure 4 shows the cyclic

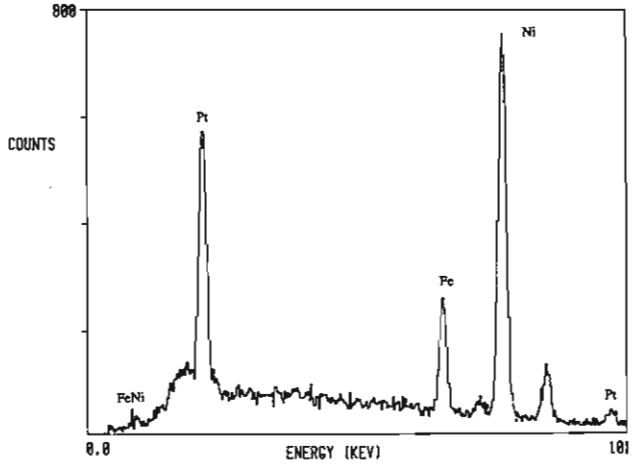

Figure 2. EDX analysis of a Ni electrode derivatized in $[Pt(NH_3)_4]_2I$ as described in the text, confirming the presence of Pt in the surface-confined species.

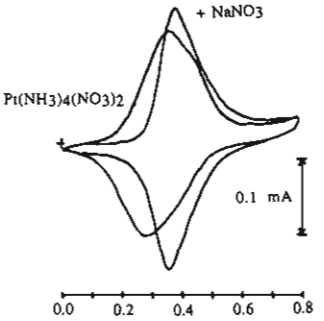

Figure 3. Cyclic voltammograms of a nickel ferrocyanide derivatized electrode (coverage= 1.3×10^{-9} mol/cm^2) in 1 M $NaNO_3$ supporting electrolyte (narrow peak) and in 1 M $[Pt(NH_3)_4](NO_3)_2$ supporting electrolyte (broad peak) at a scan rate of 100 mV/s.

voltammograms for an identical nickel ferrocyanide electrode in 1 M $NaNO_3$ supporting electrolyte before and after the addition of Pt(II) to the solution. A new redox event is observed to grow in as a shoulder of the original peak at a potential of ~0.68 V vs SCE while the original peak diminishes in size as a function of time. This new peak can be attributed to the complex of interest, as discussed below. In situ synthesis of Ni_2I on the electrode surface always leads to an interface containing unreacted nickel ferrocyanide, as evidenced electrochemically by the continued prominence of the redox wave at about ~0.35 V vs SCE. Also, the total charge passed electrochemically has diminished during the course of the chemical transformation, indicating that some of the film has dissolved or become inactive. Therefore, it was desirable to synthesize a pure bulk sample of $[Pt(NH_3)_4]_2I$ and to then attach it directly to the native nickel electrode surface under anodizing conditions known to produce a near-electrode population of Ni^{2+} ions.

Evidence that the anion I is chemically attached to a nickel electrode that has been anodized in its presence for 3 min at 1.2 V vs SCE is provided by spectroscopic and electrochemical diagnostics. Prominent infrared absorptions of the species in the powder form, as a nickelous precipitate, and on an electrode surface are listed in Table I and assigned by analogy with previously reported complexes.[6] The oxidation states of the iron and platinum moieties of $[Pt(NH_3)_4]_2I$ have been assigned previously[5] and were determined to be "$Fe^{II}/Pt^{IV}/Fe^{II}$." The cyanide stretching region between 2000 and 2200 cm^{-1} contains absorptions corresponding to bridging and nonbridging ν(CN) vibrations for the solid sample, in agreement with the previously reported single crystal X-ray structure.[5] On the electrode surface, as well as in the bulk nickel precipitated complex, a single absorption at about

(6) Nakamoto, K. *Infrared and Raman Spectra of Inorganic Coordination Compounds*, 4th ed.; John Wiley and Sons: New York, 1986; p 272.

Table I. Selected Infrared Frequencies (cm^{-1}) and Their Assignments for $[Pt(NH_3)_4]_2I$ and Related Compounds in the Form of KBr Pellets unless Otherwise Noted

	IR frequency					
assignt	$[Pt(NH_3)_4]_2I$	$[Pt(NH_3)_4]Cl_2$[a]	$[Pt(NH_3)_6]Cl_4$[a]	Ni_2I	I on Ni[b]	I on SnO_2[b]
$\nu_a(NH)$	3230	3236	3150	3242	3196	3198
$\nu(CN)$	2123, 2052 t			2070	2073	2068
$\delta(HNH)$	1388, 1345 t	1325	1370	1384, 1348 w	1382, 1310	1388, 1316
$\rho_r(NH_3)$	975, 875	842	950	*e*	950	955
$\nu(MC)$	583, 558			589, 561	*e*	*e*
$\nu(MN)$	511	510	530, 516	*e*	532[c]	534[c]
$\nu(MN)-(R)$[d]	563, 542	524, 508	569, 545	*e*	*e*	*e*

[a] Reference 6, p 191. [b] Surface derivative. [c] $\nu(MN)$ assigned for M-NC unit. [d] Raman mode. [e] Not assigned.

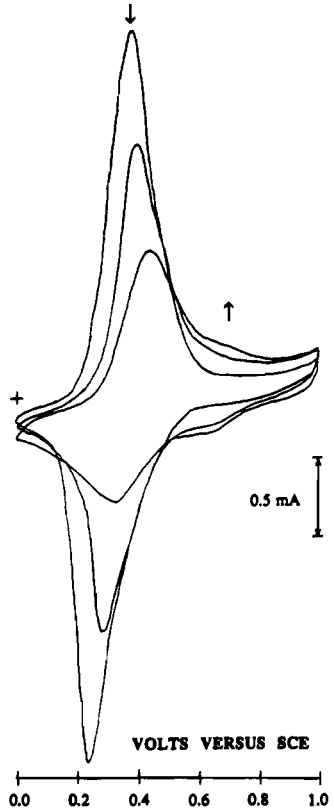

Figure 4. Cyclic voltammogram of a nickel ferrocyanide derivatized electrode (coverage= 1.4×10^{-8} mol/cm^2) whose potential was cycled in a solution containing 1 M $NaNO_3$ and 1 M $[Pt(NH_3)_4](NO_3)_2$ at a scan rate of 200 mV/s. The arrows indicate changes associated with the shapes of the redox waves as a function of time, attributed to the formation of a new complex on the electrode's surface.

2070 cm^{-1} is observed and is assigned to a complex containing all bridging iron(II) cyanides. Bridging cyanide absorptions have a well-documented literature for occurring at higher energy than their nonbridging counterparts[6] due to removal of electron density from the cyanide $2p\pi^*$ orbital, making it a weaker back-bonder to the metal. The effect is less dramatic in octahedral species containing all six bridging ligands as opposed to those containing only one bridging CN. In the latter case, the strong M–C bond of a nonbridging CN further weakens the back-bonding of the trans bridging CN, thereby increasing ν(bridging CN) more so than in the former case. This explains the difference in energy between the assigned ν(bridging Fe(II) CN) for the singly bridged starting complex $[Pt(NH_3)_4]_2I$ (2123 cm^{-1}) and the completely bridged (via Ni^{2+}) surface species (2073 cm^{-1}). The latter value closely resembles that of Prussian Blue (2080 cm^{-1}),[7] which has an analogous structure containing entirely bridging Fe(II) cyanides. Infrared cyanide stretching frequencies for ferri- and ferrocyanide derivatized on nickel are shown in Table II, with ν(CN) values of 2164 and 2091 cm^{-1}, respectively. A comparison

Table II. Selected Diffuse-Reflectance Infrared Frequencies (cm^{-1}) for $[Pt(NH_3)_4]_2I$ and Related Species on a Nickel Surface

compd	ν(CN)	compd	ν(CN)
$Ni[Fe(CN)_6]^{-}$[a]	2164	Ni_2I	2073
$Ni[Fe(CN)_6]^{2-}$[a]	2091	Ni_2I after photolysis	2146, 2093

[a] Reference 2.

of this data indicates that the observed surface species contains its iron moieties in the same oxidation state as in the reported single crystal structure. Comparison of the ν(MC) stretching frequencies of $[Pt(NH_3)_4]_2I$ and its nickel precipitate (see Table I) further supports this conclusion.

The ammine infrared bands of $[Pt(NH_3)_4]_2I$ and its surface analogue at approximately 1400 cm^{-1}, which are assigned to ν_s(HNH), also serve to demonstrate that the desired compound is surface attached as an intact trinuclear species. By comparison with the reported ammineplatinum complexes in Table I, oxidation states of Pt(II) and Pt(IV) can be observed for $[Pt(NH_3)_4]_2I$, in agreement with the presence of two $Pt^{II}(NH_3)_4^{2+}$ counterions and a central Pt(IV) unit of the trinuclear anion (as previously reported). However, in the surface-attached species, only Pt(IV) is observed, as expected, since the Pt(II) counterions have now been replaced by the electrogenerated Ni(II) ions. This species is structurally composed of the Fe–Pt–Fe units bound by the Ni counterions via the lone pairs on the cyano nitrogen atoms, thereby containing only bridging cyanide stretches in the cyanide stretching region of the infrared.

The electrochemistry of the surface-attached complex was examined by using cyclic voltammetry. The solution electrochemistry of $[Pt(NH_3)_4]_2I$ has been previously reported.[5] The cyclic voltammogram for the nickel-derivatized species generally shows two redox events occurring at 0.42 and 0.68 V vs SCE in 1 M $NaNO_3$. The first (ranging from 0 to 50% of the latter peak's anodic peak current) has been eliminated on several occasions depending on the exact derivatization technique and solution (solutions that have been standing for a number of days decompose photochemically to generate ferricyanide[5]), thereby demonstrating its presence to be an impurity. We have assigned this redox wave to the surface-confined $[NiFe(CN)_6]^{2-/-}$ couple, which has been reported to occur at 0.36 V when scanned in 1 M $NaNO_3$ supporting electrolyte.[1] The more positive wave is assigned to surface-attached I; the 80-mV positive shift of this peak when compared to that for the solution species is not surprising in light of the previously reported behavior of surface-attached nickel ferrocyanide (0.21–0.36 V vs SCE). This redox potential shift is probably due to the formation of the nickel complex, not simply the confinement of the species to the electrode. The proximity of the $E_{1/2}$ values for the two species further supports the conclusion that the surface material has not undergone a major chemical transformation upon reaction with the electrode surface. As expected for a nondiffusive, surface-confined species, the observed peak current is found to be directly proportional to the scan rate[8] (Figure 5) for scan rates ranging from 50 to 300 mV/s.

Powder X-ray diffraction of the derivatized material of interest on nickel foil electrodes in the 2θ range 16–46° shows only a

(7) Ghosh, S. N. *J. Inorg Nucl. Chem.* **1974**, *36*, 2465.

(8) Nicholson, R. S.; Shain, I. *Anal. Chem.* **1964**, 36, 706.

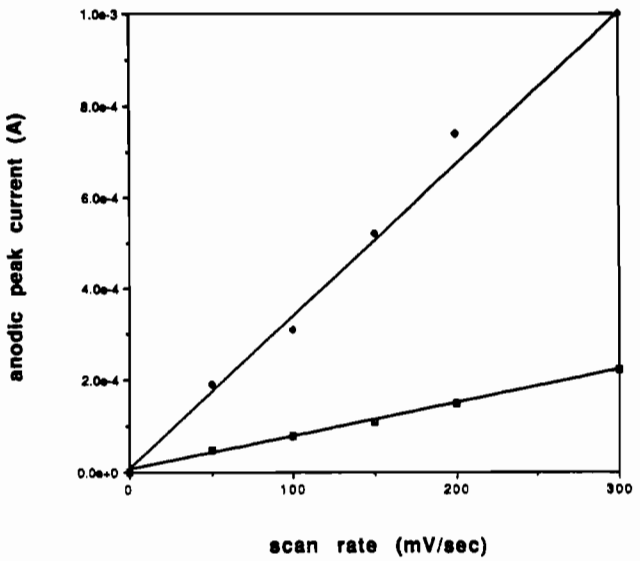

Figure 5. Scan rate dependence of the anodic peak current of a Ni electrode derivatized in $[Pt(NH_3)_4]_2I$ whose potential was cycled in 1 M $NaNO_3$ over the scan rate range of 50–300 mV/s.

Table III. Redox Properties of a Nickel Electrode Derivatized with (A) Ferricyanide,[a] (B) I, and (C) I after Irradiation at 488 nm[b]

cation	E_{ox}	E_{red}	ΔE	$E_{1/2}$
		(A) $[NiFe(CN)_6]^{2-/-}$		
Na	0.42	0.30	0.12	0.36
K	0.51	0.42	0.09	0.47
Rb	0.72	0.61	0.11	0.67
Cs	0.80	0.67	0.13	0.74
		(B) Ni_2I		
Na	0.48, 0.74	0.36, 0.63	0.12, 0.11	0.42, 0.68
K	0.53, 0.75	0.40, 0.61	0.13, 0.14	0.47, 0.68
Rb	0.82	0.69	0.13	0.76
Cs	0.86	0.77	0.09	0.82
		(C) Ni_2I (Photolyzed)		
Na	0.41	0.37	0.04	0.39
K	0.54	0.48	0.06	0.51
Rb	0.70	0.59	0.11	0.65
Cs	0.77	0.65	0.12	0.71

[a] Data taken from ref 2. [b] All potentials are in volts versus SCE and are cycled in 1 M nitrate solutions of the respective cation.

powder pattern corresponding to nickel metal (2θ = 44.6°), suggesting that the current system is best described as an noncrystalline interfacial layer. Previous powder X-ray diffraction work in our laboratory has demonstrated the microcrystallinity of the nickel ferrocyanide derivatized nickel electrode.[9] A further discussion of this point is given in the following section. As seen in Table IIIB, the redox potential of the derivatized surface does not vary significantly with that for the intercalated cation when compared to the 600-mV shift in potential of the nickel ferrocyanide surface between Li^+ and Cs^+ intercalation (see Table IIIA). Of the cyanometalate-derivatized electrodes we have previously studied, those that are noncrystalline[10,11] have not yielded the strong cation dependence observed for $NiFe(CN)_6^{2-/-}$.[2]

Photochemistry. The photochemistry of $[Pt(NH_3)_4]_2I$ in solution has been reported previously.[5] This complex exhibits a broad intervalent (IT) charge-transfer band corresponding to the metal-to-metal charge transfer between Fe(II) and Pt(IV), centered at 424 nm. Irradiation into this absorption effects a net two-electron charge transfer, generating 2 mol of ferricyanide and 1 mol of tetraammineplatinum(II) for every mol of $[Pt(NH_3)_4]_2I$

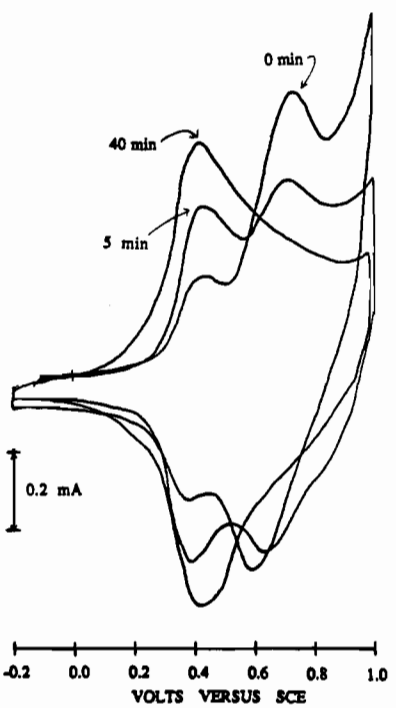

Figure 6. In situ cyclic voltammograms of a Ni electrode derivatized in $[Pt(NH_3)_4]_2I$ (coverage= 3.2×10^{-9} and 3.2×10^{-10} mol/cm^2 before irradiation and 2.8×10^{-10} and 6.5×10^{-10} mol/cm^2 after irradiation for the $[NiFe(CN)_6]^{2-/-}$ and Ni_2I peaks, respectively) and whose potential was cycled in 1 M $NaNO_3$ at a scan rate of 200 mV/s after 0, 5, and 40 min of irradiation at 488 nm.

photolyzed. The derivatized material Ni_2I appears red or orange in color (depending on the amount deposited) and is qualitatively much more intense in color than an equivalently derivatized amount of nickel ferrocyanide, which is light yellow in color. In fact, it was this intense reddish hue that led to the initial discovery of the complex while the potential of a nickel ferrocyanide electrode was cycled in a Pt(II) solution. Irradiation of the derivatized electrode in air at 488 nm (1 W, 1.5 mm Ar^+ ion laser beam) for several minutes leads to loss of the red color and the formation of a much less intense yellow surface. FTIR diffuse reflectance of the resulting surfaces consistently yields two ν(CN) peaks at about 2146 and 2093 cm^{-1}. Comparison with the surface CN stretching frequencies of ferro- and ferricyanide in Table II indicates a correspondence to a mixture of all-bridging iron(II) and iron(III) cyanides. Several electrodes tested yielded only the latter peak, corresponding to the ferrous oxidation state. In analogy with the reported observation for the nickel ferro/ferricyanide electrode in which the oxidized form of the electrode rapidly reverts to the ferrous state[2] and in comparison to the observed solution photochemistry,[5] we postulate the reaction to occur as follows. The photoinduced charge-transfer reaction occurs as in solution, generating 2 mol of ferricyanide and 1 mol of Pt(II). The Pt moiety is not coordinatively bound as evidenced by the change in stretching frequencies of the cyanide stretches (but is still present as indicated by the presence of amine stretches), whereas the iron units remain bonded to the Ni surface via attachment through the lone pairs of the cyano group nitrogen atoms. Therefore, the resultant surface consists essentially of nickel ferricyanide, which, as mentioned above, is subject to reduction by nickel metal, converting to the Fe(II) oxidation state. In this manner, the photolyzed ν(CN) peaks at 2146 and 2093 cm^{-1} can be assigned as a combination of the bridging iron(III) cyanides resulting from the initial photolysis and the bridging iron(II) cyanides resulting from the thermal reduction process, respectively. The electrodes containing only the latter peak can be explained as having completely reverted to the Fe(II) oxidation state.

Further evidence that the solution and surface photochemistry are related is provided by the resultant electrochemistry of the photolyzed electrode. Figure 6 depicts the effect of in situ pho-

(9) Amos, L. J. Ph.D. Thesis, Princeton University, 1988.
(10) Sinha, S.; Humphrey, B. D.; Fu, E.; Bocarsly, A. B. *J. Electroanal. Chem. Interfacial Electrochem.* **1984**, *162*, 351.
(11) Hidlago-Luangdilok, C.; Bocarsly, A. B. *J. Phys. Chem.* **1990**, *94*, 1918.

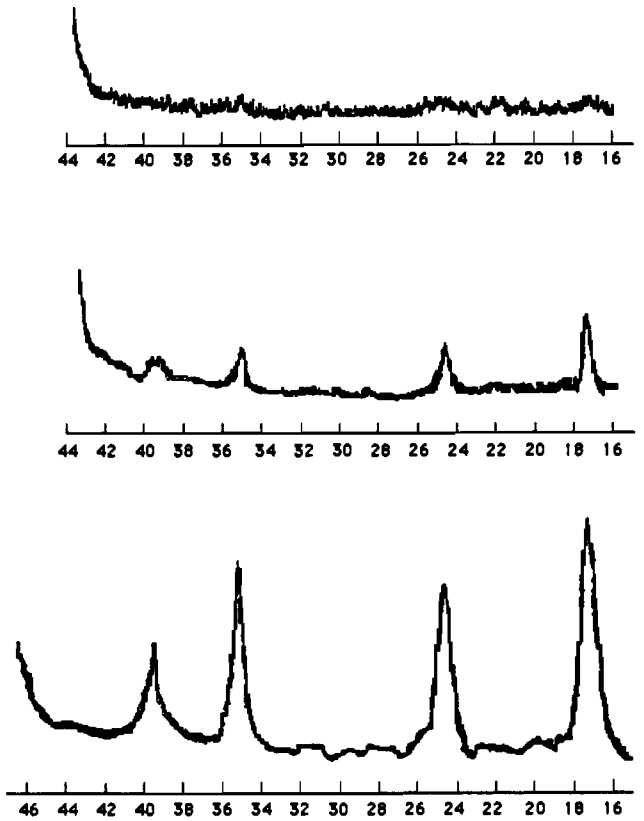

Figure 7. Powder X-ray diffraction patterns of a Ni_2I-derivatized electrode (a) stored in the dark, (b) exposed to room light for several hours, and (c) irradiated for 1 h at 488 nm with an Ar^+ ion laser. 2θ values for the observed peaks are listed in the text.

tolysis on the cyclic voltammograms of the surface species in 1 M $NaNO_3$. It can be seen from this figure that the $[NiFe(CN)_6]^{2-/-}$ peak at 0.42 V vs SCE increases in size as a function of photolysis time while the redox peak at 0.68 V vs SCE associated with the oxidation of surface-attached Ni_2I decreases as the photolysis proceeds. The number of redox-active centers has also diminished during the course of photolysis as described in the figure caption. Parallel experiments in which the photolyzed interfacial layer was monitored by X-ray powder patterns indicate the growth of diffraction peaks as shown in Figure 7. From these data, it can be seen that the noncrystalline Ni_2I interface (see Figure 7a) is converted to a crystalline form as the photolysis proceeds. The observed powder pattern corresponds well with those previously obtained for authentic interfacial layers and bulk samples[9] of $[NiFe(CN)_6]^{2-/-}$ (2θ = 17.34, 24.73, 35.24, and 39.60°). This pattern is consistent with the formation of a cubic lattice. The observed pattern cannot be accounted for by using the available single-crystal data for $[Pt(NH_3)_4]_2I$,[5] which crystallizes in a monoclinic unit cell. By analogy with $[NiFe(CN)_6]^{2-/-}$ and Prussian Blue, the observed diffraction peaks are indexed to the following Miller indices (in parentheses): 2θ = 17.34° (200), 2θ = 24.63° (220), 2θ = 35.14° (400), and 2θ = 39.40° (420). Thus, the surface photolysis product is unambiguously identified as microcrystalline $[NiFe(CN)_6]^{2-/-}$ by X-ray powder pattern, IR spectroscopy, and cyclic voltammetric data.

Whereas the anodic peak potential of the Ni_2I oxidation is relatively independent of the intercalated cation compared to that of $[NiFe(CN)_6]^{2-/-}$ (see Figure 8 and Table IIIB), the photolysis product peak (i.e. the anodic peak centered at 0.42 V vs SCE) varies greatly with the counterbalancing cation. Figure 9 shows the cyclic voltammograms for the photolyzed electrode in 1 M nitrate solutions of Na, K, Rb, and Cs. Comparison of Table IIIA,C for the $E_{1/2}$ values of a nickel ferrocyanide electrode to those for the photolyzed electrode of interest in various alkali-metal cation solutions shows that the redox potentials of these two surface species are nearly identical. This further corroborates the available evidence that one can generate a surface-confined nickel ferrocyanide lattice photochemically from an electrode initially derivatized in $[Pt(NH_3)_4]_2I$.

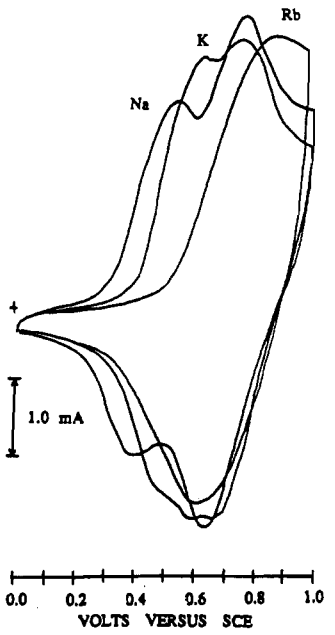

Figure 8. Cyclic voltammograms of a Ni electrode derivatized in $[Pt(NH_3)_4]_2I$ (coverage = 9.7×10^{-10} and 6.4×10^{-10} mol/cm^2 for the $[NiFe(CN)_6]^{2-/-}$ and Ni_2I peaks, respectively) whose potential was cycled in 1 M solutions of sodium, potassium, and rubidium nitrate as labeled in the diagram at a scan rate of 200 mV/s.

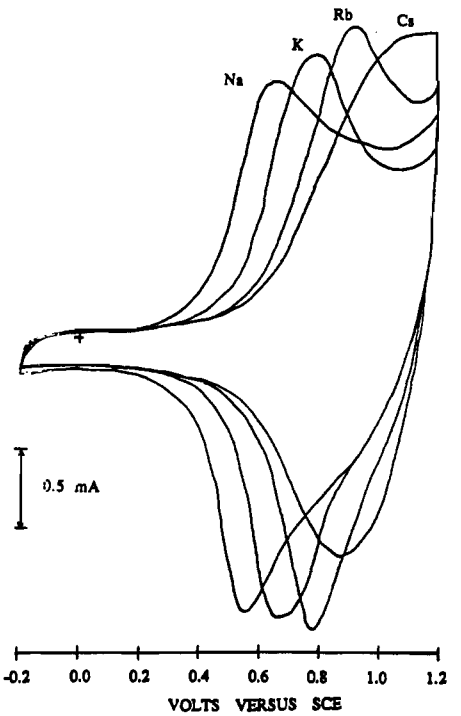

Figure 9. Cyclic voltammograms of a photolyzed (488 nm) Ni_2I-derivatized electrode (coverage = 5.0×10^{-9} mol/cm^2) whose potential was cycled in 1 M of solutions of sodium, potassium, rubidium, and cesium nitrate as labeled in the diagram at a scan rate of 200 mV/s.

The photolytic conversion of the noncrystalline surface Ni_2I, which does not show a significant cation dependence on redox potential, into a microcrystalline nickel ferrocyanide lattice, which is cation dependent, provides the first direct evidence that a well-ordered, microcrystalline lattice is necessary to produce the observed cation effect. We have previously postulated that the effect of the intercalated alkali-metal cation in the nickel ferrocyanide derivatized surface on the redox potential of the attached iron species is structural in nature since evidence[2,3,9-11] indirectly suggests that introduction of different alkali-metal cations into

the surface lattice causes a distortion of the crystal field felt by the iron centers. The photochemical generation of this ordered morphology from an noncrystalline, cation-independent one further supports this hypothesis.

The energetic design of the modified electrode interface can be contoured in a very specific manner by taking advantage of the presence of two structurally distinctive domains on the electrode surface. This can have important consequences with respect to the development of reaction specific, electrocatalytic interfaces. Within the context of the current system, the details of the surface free energy differential between domains can be controlled by taking advantage of the observed variation in cation effects associated with the two electrode confined species. As shown in Figure 8, the presence of one surface species that has a strong dependence of $E_{1/2}$ on the intercalated cation ($[NiFe(CN)_6]^{2-/-}$) and one species in which $E_{1/2}$ is only slightly dependent on the supporting electrolyte cation (Ni_2I) allows one to adjust the free energy difference between these two domains by the selection of supporting electrolyte. Thus when Na^+ is intercalated into the surface layer, one obtains two anodic cyclic voltammetric events separated by ~250 mV. However, in the presence of Rb^+ cations, the $[NiFe(CN)_6]^{2-/-}$ wave is shifted sufficiently positive so that it overlaps the Ni_2I wave; thus, both domains are oxidized simultaneously. Hence, in the present multistructural system, potential control, in conjunction with cation-induced structural control, allows one to control the number of electrons that flow per stoichiometric unit as well as the differential free energy $[\Delta(\Delta G)]$ of the charge-transfer process. Note that while one might achieve the same sort of effect by simply having two chemically distinct species (not having microstructure-related redox events) on an electrode surface, it would be impossible to adjust the differential potential dependence of the two surface species once the electrode interface was synthesized. In addition to the potential and stoichiometric control indicated above, if it is hypothesized that the two types of structural domains present on the electrode must be spatially segregated (this assumption may not be true), then the application of different intercalates and potentials allows one to spatially control the charge-transfer process. Thus, in the presence of Na^+ ions, the two distinct redox events would occur at different locations in the derivatizing layer, while in the presence of Rb^+ a fairly homogeneous charge-tranfer process is imagined. Whether or not this latter type of spatial charge-transfer control occurs in the system of present interest is the subject of continued study.

Electropolymerization. If $\{[Pt(NH_3)_4]_2^{4+}\}\{[(NC)_5Fe^{II}(CN)Pt^{IV}(NH_3)_4(NC)Fe^{II}(CN)_5]^{4-}\}$ is oxidized at an inert electrode (at 1.4 V vs SCE) such as SnO_2 or Pt, which is incapable of undergoing anodic dissolution to generate soluble metal ions, an interfacial surface layer is still observed. Fairly high concentrations of $[Pt(NH_3)_4]_2I$ (~50 mM) are required to see this effect. No surface species is formed by simply soaking the electrode in a solution of $[Pt(NH_3)_4]_2I$ or by holding the electrode at potentials negative of the known solution redox potential for the oxidation of "$[Fe^{II}Pt^{IV}Fe^{II}]^{4-}$" to "$[Fe^{III}Pt^{IV}Fe^{III}]^{2-}$." Furthermore, if the Pt(II) counterions in $[Pt(NH_3)_4]_2I$ are cation exchanged for K^+, no surface species is observed. Also, no surface species is formed on SnO_2 when potassium ferricyanide is substituted for $[Pt(NH_3)_4]_2I$ as the derivatization agent. On the basis of these data, it is concluded that complex $[Pt(NH_3)_4]_2I$ can be oxidized to generate an inorganic polymer consisting of repeating "$[Pt^{IV}Fe^{II}]$" units. Unlike the material discussed in the previous sections, this inorganic polymer is not "cemented" together by cyanide bridges to a third coordinated metal (i.e Ni^{2+}); rather, it is a simple repetition of the molecular structure associated with compound I as shown below.

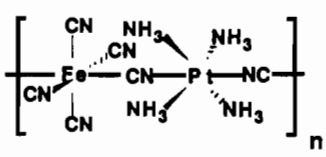

Whether the polymer is linear or branched is unclear at this time.

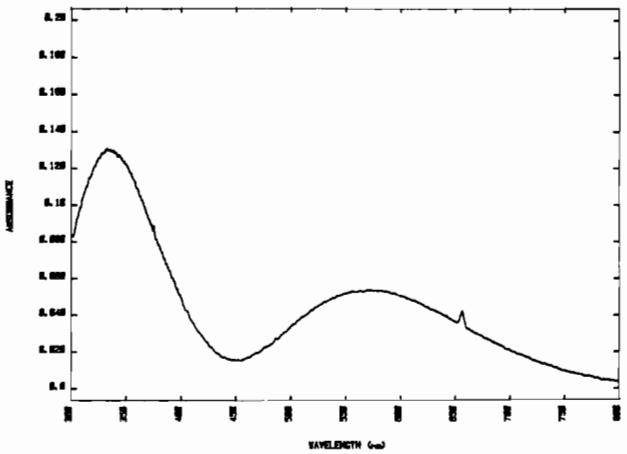

Figure 10. UV–vis absorption spectrum of the electropolymerized form of I on a SnO_2 on glass electrode referenced against unmodified SnO_2 on glass.

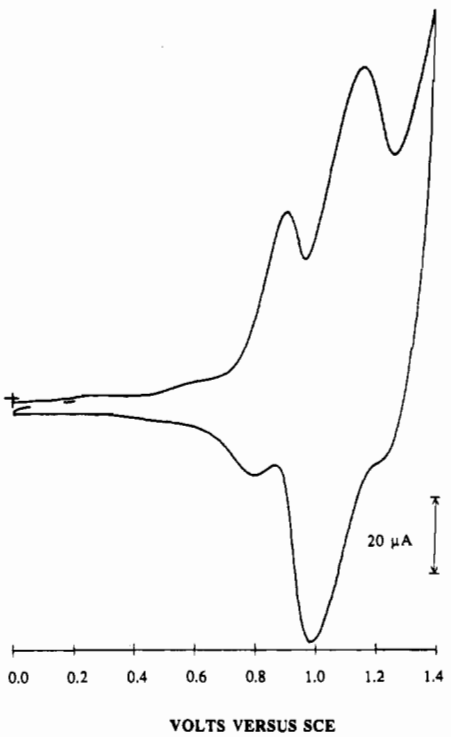

Figure 11. Cyclic voltammogram of the electropolymerized form of I on a SnO_2 on glass electrode (coverage = 2.1×10^{-9} mol/cm^2, assuming one electron is transferred per peak) whose potential was cycled in 1 M $NaNO_3$ at a scan rate of 25 mV/s.

Also the degree of cross-linking has not been ascertained. The UV–vis absorption spectra of the polymeric species on SnO_2 (referenced against underivatized SnO_2 on glass) is shown in Figure 10. Two broad peaks occur, centered around 337 and 570 nm. The exact positions of these two peaks vary (up to 40 nm) with different electrode samples, depending on the length of derivatization time, concentration of derivatization solution, and applied potential. This may indicate different polymer chain lengths or degrees of crosslinking. The high-energy peak is preliminarily assigned as MLCT {Fe(II) → Π*(CN)} by analogy with the spectrum of $Fe(CN)_6^{4-}$, while the second is attributed to the intervalent charge transfer between Fe(II) and Pt(IV), in analogy with the previously reported electronic assignments for $[Pt(NH_3)_4]_2I$[5]. Both peaks are red-shifted in energy from the "monomeric" complex ($[Pt(NH_3)_4]_2I$), a result that may be due to an increasing degree of delocalization with chain length.

Diffuse-reflectance FTIR spectra of the polymer-coated surfaces in the cyanide stretching region yielded one broad cyanide stretch between 2060 and 2080 cm^{-1}, with the average being 2068 cm^{-1}.

These results indicate that there is only one form of CN^- present in the polymerized derivative and that a majority of the cyanide ligands are bridging in nature. Both the oxidation state of the Fe moiety and the fact that the surface complex contains mainly bridging $\nu(CN)$ add further support for the assignment of this species as the $[Fe^{II}Pt^{IV}]_n$ polymer. The presence of Pt(IV) on the surface is confirmed by analogy to other ammineplatinum compounds as shown in Table I. The ammine assignments are likewise very similar to those reported for Ni_2I on the Ni surface, all corresponding to the Pt(IV) oxidation state.

Cyclic voltammograms of the electropolymerized species on SnO_2 (using derivatization times of less than 30 s) show two quasireversible redox waves (see Figure 11) in 1 M $NaNO_3$, occurring at 0.86 and 1.09 V vs SCE. These peaks are not cation dependent. As in the case of the nickel complex, no X-ray powder diffraction peaks are observed that can be attributed to the polymer. Thus, it appears that the polymerized surface species does not form a crystalline lattice. If longer derivatization times are employed, only one cyclic voltammetric peak is observed prior to the anodic solvent window cutoff. The exact reasons for these dissimilar results are the subject of continued study.[12]

The above results merit a reevaluation of the electrochemistry of Ni_2I on a Ni surface since the cyclic voltammetric peaks of this complex might also be explained in terms of electropolymerization of $[Pt(NH_3)_4]_2I$ on Ni. However, control experiments utilizing a nickel working electrode with the K^+-exchanged complex K_4I demonstrated that an interfacial layer is still formed on the Ni surface. This interface yielded a cyclic voltammogram in 1 M $NaNO_3$ which was identical with that obtained for Ni_2I on Ni. In addition, a comparison of the UV-vis spectroscopy of the Ni_2I on nickel-plated SnO_2 vs the polymerized complex shows a shift in the IT band from 416 to 570 nm. Therefore, one can conclude that the reported chemistry of $[Pt(NH_3)_4]_2I$ at a Ni surface is distinctly different from that at SnO_2 or Pt. In the former case, $[Pt(NH_3)_4]_2I$ preferentially forms a Ni(II) precipitate, whereas electropolymerization occurs at the latter electrodes.

The following mechanism is postulated for the formation of the polymerized interfacial structure. Oxidation of "$[Fe^{II}Pt^{IV}Fe^{II}]^{4-}$" at a potential of 1.4 V vs SCE generates "$[Fe^{III}Pt^{IV}Fe^{III}]^{2-}$." This species can then oxidize one of the $Pt(NH_3)_4^{2+}$ counterions to form the polymeric chain "$[Fe^{II}Pt^{IV}]_n$" as depicted below. Reoxidation of "$[Fe^{II}Pt^{IV}]_n$" allows for further chain growth:

$$n\mathrm{Fe^{II}Pt^{IV}Fe^{II}} \rightarrow n\mathrm{Fe^{III}Pt^{IV}Fe^{III}} + 2ne^- \quad (1)$$

$$n\mathrm{Fe^{III}Pt^{IV}Fe^{III}} + n\mathrm{Pt^{II}} \rightarrow [\mathrm{Fe^{II}Pt^{IV}}]_{2n} \quad (2)$$

$$[\mathrm{Fe^{II}Pt^{IV}}]_{2n} \rightarrow [\mathrm{Fe^{III}Pt^{IV}}]_{2n} + 2ne^- \quad (3)$$

$$[\mathrm{Fe^{III}Pt^{IV}}]_{2n} + \mathrm{Pt^{II}} \rightarrow [\mathrm{Fe^{II}Pt^{IV}}]_{2n+1} \quad (4)$$

Acknowledgment. This work was supported by the National Science Foundation under Grant No. CHE-8700868. We thank M. Zhou and J. L. Steiger for technical assistance and valuable discussions.

(12) While a shift in redox potential with organic polymer chain length is not to be expected, the coordination chemistry of the described inorganic "polymer" dictates that such a relationship should exist. Specifically, in the present case, polymer chain and/or degree of branching is related to the number of terminal versus bridging cyanide ligands. It has previously been reported[13] that the redox potential of cyanometalate complexes is strongly dependent on the environment of the cyanide nitrogen lone pair. Thus, even moderate changes in the solvent environment can have a dramatic effect on redox potential.[14] Therefore, the observed redox potential for the polymer should be a strong function of the ratio of terminal cyanides to cyanides in which the nitrogen forms a dative bond.

(13) Gutmann, V.; Gritzner, G.; Danksagmüller, K. *Inorg. Chim. Acta* **1976** *17*, 81.

(14) Gritzner, G.; Danksagmüller, K.; Gutmann, V. *J. Electroanal. Chem. Interfacial Electrochem.* **1976**, *72*, 177.

Contribution from the Chemistry and Physics Laboratory, The Aerospace Corporation, El Segundo, California 90245, and Department of Physics, University of California, Riverside, California 92521

Photoelectron Spectroscopic Studies of the Electronic Structure of α-SiC

Stephen V. Didziulis,*[†] Jeffrey R. Lince,[†] Paul D. Fleischauer,[†] and Jory A. Yarmoff[‡]

Received April 4, 1990

The electronic structure of single-crystal α-SiC (silicon carbide) has been determined with variable photon energy valence band photoelectron spectroscopy. Synchrotron radiation in the range 30-250 eV was used in addition to a conventional Al Kα X-ray source to follow the intensity changes of valence band features as a function of the incident photon energy. The dominant atomic orbital contributions have been assigned to valence band features by comparing them to theoretical atomic photoionization cross sections. The results indicate that C 2s based ionizations appear at the highest binding energy, near 15 eV, while Si 3s features are evident near 10 eV. The highest occupied energy levels (from approximately 1-8-eV binding energies) are predominantly C 2p based. Differences between the photon energy dependence of the data and theoretical atomic orbital cross sections show the valence levels to be highly mixed. Comparison of the valence band spectra with a molecular orbital calculation confirms the experimental assignments, but the calculation appears to underestimate the extent of atomic orbital mixing. The valence band spectrum of a hot-pressed polycrystalline SiC sample compares quite well with the single-crystal spectrum. The implications of these results on the chemisorption behavior and reactivity of SiC are discussed.

Introduction

Silicon carbide (SiC) has attracted interest for electronic applications as a possible hostile environment semiconductor and for tribological applications as an abrasive and as a candidate for wear-resistant mechanical parts. SiC is an excellent candidate for all these applications because of its high hardness, high melting point, and relative chemical inertness. Despite the interest shown in SiC, little experimental work has been performed to determine its electronic structure.[1-5] The work presented in this paper uses variable photon energy valence band photoelectron spectroscopy (PES) to study the electronic structure of α-SiC.

Electronic structure is of obvious importance in electronic applications, which require high-purity materials for device production. In this regard, SiC poses a problem, however, because it grows in a variety of crystal structures. The wurtzite (or α) phase is easiest to grow but exists in over 100 different polytypes, which actually consist of mixtures of hexagonal and cubic packing.

[†] The Aerospace Corp.
[‡] University of California.

(1) Hoechst, H.; Tang, M.; Johnson, B. C.; Meese, J. M.; Zajac, G. W.; Fleisch, T. H. *J. Vac. Sci. Technol., A* **1987**, *5*, 1640.
(2) Sasaki, T. A.; Baba, Y. JAERI-M Report 85-063; Japan Atomic Energy Research Institute: Tokai-Mura, Japan, 1985.
(3) Xu, X.; Zhang, F.; Chen, G. *J. Non-Cryst. Solids* **1987**, *90*, 295.
(4) Parrill, T. M.; Bermudez, V. M. *Solid State Commun.* **1987**, *63*, 231.
(5) Fang, R.-C.; Ley, L. *Phys. Rev. B* **1989**, *40*, 3818.

0020-1669/91/1330-0672$02.50/0 © 1991 American Chemical Society